High temperature corrosion of low and high alloy steels under molten carbonate fuel cell conditions

Hochtemperaturkorrosion von niedrig- und hochlegierten Stählen unter Schmelzkarbonat-Brennstoffzellenbedingungen

P. Biedenkopf*, M. Spiegel and H. J. Grabke

Dedicated to Dr. U. Heubner on the occasion of his 65th birthday

The corrosion behavior of eight low and high alloy steels was investigated under simulating the conditions at the cathode of a molten carbonate fuel cell at 650 °C. Different Li-containing iron oxides ($LiFeO_2$ and $LiFe_5O_8$) were formed in contact with the eutectic (Li, K)-carbonate melt depending on the Cr-content of the steel. These oxides show low solubility in the melt and protect the metallic material against further corrosive attack. Fast growing scales of Fe_3O_4 and $LiFe_5O_8$ were observed on the low alloy ferritic steel 10 CrMo 9 10. Higher alloy steels form $LiFeO_2$ in contact with the melt and mixed Fe-Cr-spinels underneath. Steels with Cr-contents over 20 wt.% Cr form a mixed $LiCr_{1-x}Fe_xO_2$ and $LiCrO_2$ layer in contact with the metal. Marker experiments on the commercial steel 1.4404 (X2 CrNiMo 17 13 2) show that the outer $LiFeO_2$ layer grows mainly by outward diffusion of iron ions (Fe^{3+}), whereas the inner $(Fe,Ni)Cr_2O_4$ spinel layer grows inward. After 500 hours, $LiFe_5O_8$ was formed between the spinel and the $LiFeO_2$ layer, but it had disappeared after several thousand hours of exposure as it was fully transformed to $LiFeO_2$. Co-containing $LiFeO_2$ was found after 500 hours on the high Co-containing steel 1.4971 (X12 CrCoNi 21 20), but is not stable after several thousand hours exposure. Co diffuses outward to form a protective $LiCoO_2$ layer of a few microns in thickness. Protective Cr_2O_3 layers were not observed on steels with high Cr-content ($\geq$ 25 wt.% Cr) due to peroxide ions in the melt, which cause oxidation Cr_2O_3 and flux to chromate, which is highly soluble in the melt. Further quantitative investigations on *total corrosion* considering the chromate formation have shown that high alloy steels with high amounts of Cr form mainly K_2CrO_4.

In Auslagerungsexperimenten wurde das Korrosionsverhalten von acht niedrig- und hochlegierten Stählen unter Simulation der Bedingungen an der Kathodenseite von Schmelzkarbonat-Brennstoffzellen bei 650 °C untersucht. In Abhängigkeit vom Cr-Gehalt des geprüften Stahles bilden sich im Kontakt mit der Schmelze verschiedene Li-haltige Eisenoxide, die das metallische Material vor weiterem korrosiven Angriff der eutektischen (Li,K)-Karbonat-Schmelze schützen. Schnell wachsende Korrosionsschichten wurden auf dem niedriglegierten ferritischen Stahl 10 CrMo 9 10 beobachtet, wobei die Korrosionsschicht aus Fe_3O_4 und $LiFe_5O_8$ besteht. Korrosionsbeständigere, höherlegierte Stähle bilden eine äußere $LiFeO_2$-Schicht und darunter chromhaltige Spinelle. Auf Stählen mit hohen Cr-Gehalten ($\geq$ 20 Gew.% Cr) werden keine Fe-Cr-Spinelle mehr gebildet, sondern $LiCrO_2$ und das Mischoxid $LiCr_{1-x}Fe_xO_2$ werden als innere Korrosionsschichten nachgewiesen. Markerexperimente am Werkstoff 1.4404 (X2 CrNiMo 17 13 2) haben gezeigt, daß die $LiFeO_2$ als äußere Schicht durch Auswärtsdiffusion von Fe-Kationen wächst, während die $(Fe,Ni)Cr_2O_4$-Spinellschicht offenbar nach innen wächst. Das nach 500 h gebildete, intermediäre Oxid $LiFe_5O_8$ wird nach 5000 Versuchsstunden nicht mehr beobachtet und ist vollständig in $LiFeO_2$ umgewandelt. Auf dem stark Co-haltigen Stahl 1.4971 (X12 CrCoNi 21 20) bildet sich nach kurzen Versuchszeiten Co-haltiges $LiFeO_2$, welches jedoch bei Langzeitversuchen über mehrere tausend Stunden nicht stabil ist. Co diffundiert nach außen und bildet im Kontakt mit der Schmelze eine deckende, mehrere µm dicke $LiCoO_2$-Schicht aus. Deckende Cr_2O_3-Schutzschichten werden selbst bei hohen Cr-Gehalten über 25 Gew.% nicht beobachtet, weil Cr_2O_3-Deckschichten in der Schmelze nicht stabil sind und durch die Peroxide zu in Karbonaten leicht löslichem Chromat aufgeschlossen werden. Quantitative Analysen des Chromat-Gehaltes der Schmelze führen zur Bestimmung der *gesamten Korrosion* unter Berücksichtigung der festen und flüssigen Korrosionsprodukte. Diese Untersuchungen zur Chromatbildung zeigen weiterhin, daß auf hoch Cr-legierten Stählen überwiegend K_2CrO_4 gebildet wird.

1 Introduction

Fuel cells are energy conversion devices that convert chemical energy directly into electrical energy. The high efficiency and the low emission coefficient in the production of electrical energy make fuel cell technology an important and ecologically beneficial means of producing electrical energy [1, 2]. Several types of fuel cells have been developed in the last decades. They differ in their working temperature, in the electrolyte and in the cathode and anode materials. Acid electrolytes transport H^+ ions from the anode to the cathode, whereas basic electrolytes transport O^{2-} ions in the opposite direction. A list of fuel cells and their operating temperatures is given in Table 1.

High temperature fuel cells operate at temperatures between 600 and 1000 °C. The solid oxide fuel cell (SOFC)

* *P. Biedenkopf, M. Spiegel, H. J. Grabke*
Max-Planck-Institut für Eisenforschung GmbH
Max-Planck-Str. 1, D-40237 Düsseldorf (Germany).

 0947–5117/97/0808–0477$17.50+.50/0

Table 1. Designation and expected working temperature of different types of fuel cells

Tabelle 1. Bezeichnung und angestrebte Arbeitstemperatur verschiedener Brennstoffzellentypen

type	designation	T [°C]
PEM	Proton Exchange Membrane Fuel Cell	20–120
AFC	Alkaline Fuel Cell	60–120
PAFC	Phosphoric Acid Fuel Cell	160–220
MCFC	Molten Carbonates Fuel Cell	600–650
SOFC	Solid Oxide Fuel Cell	850–1000

works at temperatures above 800 °C and uses Y_2O_3 stabilized ZrO_2 as a solid electrolyte. The molten carbonate fuel cell (MCFC) uses several carbonate mixtures as the liquid electrolyte at an operating temperature of 650 °C. In most cases a mixture of Li_2CO_3 and K_2CO_3 is used as a basic electrolyte. Thus transport of oxide ions (O^{2-}) via carbonate ions (CO_3^{2-}) from the cathode (NiO) to the anode (Ni) is established. Gas mixtures of H_2O, H_2 and CO_2 are used in the anode side, whereas in the cathodic side mixtures of O_2 and CO_2 are used.

In the anodic area hydrogen is oxidized by the carbonate ions:

$$H_2 + CO_3^{2-} \rightleftharpoons H_2O + CO_2 + 2e^- \quad (1)$$

whereas in the cathodic area oxygen and carbon dioxide form carbonate ions:

$$\frac{1}{2}O_2 + CO_2 + 2e^- \rightleftharpoons CO_3^{2-} \quad (2)$$

The reaction that proceeds in a molten carbonate fuel cell is the oxidation of hydrogen to water:

$$H_2 + \frac{1}{2}O_2 \rightleftharpoons H_2O \quad (3)$$

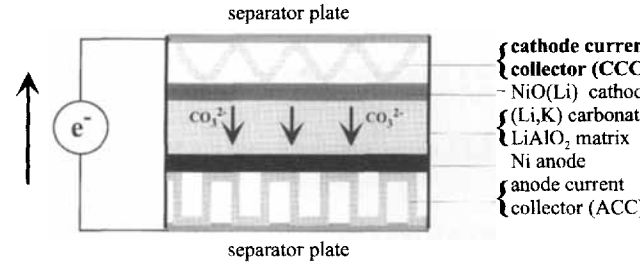

Fig. 1. Schematic model of a MCFC with electrode reactions. The $(Li_{0.62}K_{0.38})_2CO_3$-electrolyte transports carbonate-ions from the cathode to the anode side

Abb. 1. Schematischer Aufbau einer Schmelzkarbonat-Brennstoffzelle (MCFC) mit den beteiligten Elektrodenreaktionen. Der $(Li_{0.62}K_{0.38})_2CO_3$-Elektrolyt transportiert Karbonationen von der Kathoden- zur Anodenseite

One cell produces the voltages of 1 V at open circuit potential, therefore many cells must be combined to reach enough power. Several hundred cells are connected with metallic materials (separator plates) which separate the cathode from the anode gas. The flow of anode and cathode gas through the fuel cell is accomplished via hollow spaces between the cathode or anode and the current collector. Because of their good rollability and weldability metallic materials are used in MCFCs as cathode current collectors (CCC) and as separator plates between the cells (Fig. 1). The specifications for the metallic current collector are strict and can be summarized as follows [3, 4]:

- high corrosion resistance in the presence of a thin salt film and in oxidizing gas atmospheres in conjunction with low electrolyte loss by formation of ternary oxides ($LiFeO_2$ and K_2CrO_4)
- high electrical conductivity of the growing oxides to minimize the power drop of the fuel cell
- sufficient mechanical strength to maintain contact between cells at operation temperature

Table 2. Commercial steels with designation and chemical composition concerning the main alloying elements (in wt.%) [12]

Tabelle 2. Kommerzielle Stähle mit Werkstoffnummer und chemischer Zusammensetzung der Hauptbestandteile (in Gew.%) [12]

steel	designation	Cr [wt.%]	Ni [wt.%]	other elements
1.4301	X5 CrNi 18 10 AISI 304	17–19	8.5–10.5	–
1.4404	X2 CrNiMo 17 13 2 AISI 316 L	16.5–18.5	11–14	2–2.5 Mo
1.4550	X6 CrNiNb 18 10 AISI 347	17–19	8.5–10.5	Nb/Ta $\geq$ 10 × C
1.4571	X6 CrNiMoTi 17 12 2	15.5–18.5	10.5–13.5	2–2.5 Mo, $\geq$0,4 Ti
1.4845	X12 CrNi 25 21 AISI 310 S	24–26	19–22	1.5 Si
1.4877	X5 NiCrNbCe 32 27	26–28	31–33	0.6–1.0 Nb; 0.05–0.1 Ce
1.4922	X20 CrMoV 12 1	10–12.5	0.3–0.8	0.8–1.2 Mo; 0.27–1.25 V
1.4971	X12 CrCoNi 17 12 2	20–22.5	19–21	18.5–21 Co; 2.5–3.5 Mo; 2–3 W; 0.75–1.25 Nb
1.7380	10 CrMo 9 10	2–2.25		0.9–1.1 Mo
2.4642	NiCr29Fe Inconel 690	27–31	bal.	7–11 Fe, $\leq$0.5 Cu

Another less considered requirement is the solubility of the formed oxides in liquid carbonates, which should be as low as possible.

Many authors investigated the corrosion behavior of stainless steels and model alloys and the electrical conductivity of their oxide layers formed in molten carbonates. A list of steels with their international designation is given in Table 2.

Janz et al. [5, 6] tested SS347 in the ternary (Li, Na, K)$_2CO_3$ mixture at 600–700 °C with a CO_2 pressure of 1 atm. SS347 shows little corrosion and $LiFeO_2$ was the main corrosion product. *Shores* and *Singh* [7] observed a double layered oxide scale with a thickness of 5–10 µm on SS316 L after 150 h. The outer layer was mainly $LiFeO_2$ with a compact Cr_2O_3 layer at the metal/oxide interface. For thermogravimetric experiments the metallic specimens were coated with carbonates (1 mg/cm^2) and tested in cathodic gas (CO_2 und O_2). A higher corrosion resistance was observed for the stainless steel SS3105 on which a thin iron rich oxide was formed on top of a chromium rich oxide.

Corrosion tests of SS316 L and SS310 S were carried out by *Yuh* [8] on preoxidized specimens (1 h at 750 °C in O_2-CO_2-gas mixture). These specimens were tested under simulated fuel cell conditions and the amounts of Cr and Fe in the oxide scales were determinated by EDX.

The inner oxide on SS310 S contains more chromium than the inner oxide formed on SS316 L. In these tests an intermediate layer, possibly unlithiated Fe_2O_3 or Fe_3O_4 was observed on SS316 L. The preoxidized specimen showed lower electrical conductivity but higher corrosion resistance against the aggressive media. In later studies under similar conditions, *Yuh* et al. [9] identified $NiCr_2O_4$ and $FeCr_2O_4$ on SS310S by XRD.

Ghanem [10] investigated the influence of Si in thermogravimetric corrosion tests on Inconel 690, SS304 and on 5 newly developed alloys with 10–11.3 Cr, 15–18.7 Ni, 4.98–5.76 Mn, 4.18–5.52 Al and 0.36–1.5 Si at 800 °C covered with 1 mg/cm^2 Na_2CO_3/K_2CO_3 mixture. The new alloys showed better corrosion resistance than SS304, but Inconel 690 showed the best corrosion behavior. The high amounts of Al and Si were expected to be responsible for the higher corrosion resistance of the new alloys in comparison with SS304. The low corrosion is connected with a higher electrical resistance of the formed oxide scale. As already shown by *Singh* et al. [11], the electrical resistance of corrosion scales formed on Fe-Cr-Al steels is three orders of magnitude higher than scales formed on austenitic steels without Al. In later studies, *Shores* et al. [3] also reported that alloys containing sufficient Al to form Al_2O_3 or $LiAlO_2$ in contact with the melt were very corrosion resistant, but the low electrical conductivity of the corrosion products prohibits their use as a cathode current collector.

2 Experimental

Exposure tests were carried out at 650 °C under simulated molten carbonate fuel cell conditions on eight commercial steels. The ferritic and austenitic steels have Cr contents from 2.25 to 28 wt.% Cr and no Al. The composition of the steels is listed in Table 2 [12]. The setup for the exposure tests is shown in Fig. 2a and b. Metallic specimens were put on top of Ni foils which are in contact with the carbonate melt. The melt creeps through the oxidized Ni and forms a thin film of carbonate all around the specimen.

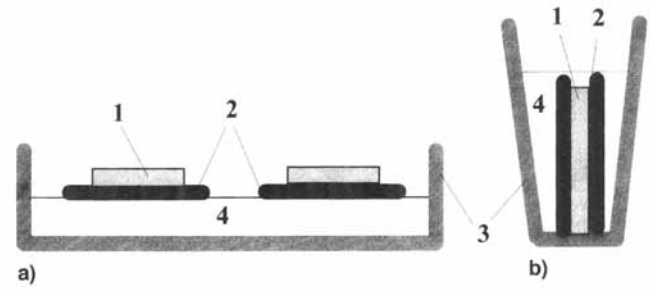

Fig. 2. Experimental setup consisting of metallic specimen (1), Ni-foils (2), Al_2O_3-crucible (3) and carbonate melt (4). The setup b) was used to investigate the total corrosion with the formation of liquid chromates

Abb. 2. Versuchsaufbau bestehend aus metallischer Probe (1), poröser Ni-Folie (2), Al_2O_3-Schälchen (3) und Karbonatschmelze (4). Versuchsaufbau b) wurde eingesetzt, um die Gesamtkorrosion unter Berücksichtigung der Chromatbildung zu untersuchen

In order to determine the corrosion kinetics, oxide scale thickness measurements were carried out on metallographic cross sections after different periods of time. The corroded specimens were investigated by optical microscopy of metallographic cross sections, X-ray diffraction (XRD), scanning electron microscope (SEM) with energy-dispersive X-ray spectroscopy (EDX) and electronprobe microanalysis (EPMA).

In the experiments a typical MCFC carbonate mixture was used consisting of 62 mol.% Li_2CO_3 and 38 mol.% K_2CO_3. This carbonate was melted, cooled, pulverized and mixed in the ratio 60:40 wt.% with $LiAlO_2$ as ceramic matrix. Subsequently the powder was filled in pure alumina crucibles and covered with porous 15 × 15 mm^2 Ni-foils (Fig. 2).

In the beginning of each experiment the carbonate melt creeps through the Ni foils and forms lithiated NiO. This lithiated NiO represents the fuel cell cathode separating the melt and the cathode current collector as in a real MCFC. Simultaneous to the formation of NiO(Li) the oxidation of the specimens begins and oxides containing no Li are formed. When the Ni foils are fully lithiated, the carbonates creep through the NiO and form a thin carbonate layer on the oxidized metal. As already shown by *Shores* and *Singh* [7], the tests with a thin film of salt give a much more realistic representation of the corrosion conditions expected on a current collector, than experiments with specimens immersed in a melt.

The specimens (10 × 10 × 3 mm^3) were ground through 600 grit SiC paper on all sides, washed with ethanol and placed on top of the Ni foils (Fig. 2). The crucibles with the specimens were put in the furnace and the reaction time was recorded after the temperature of 650 °C was reached. After 50, 100, 200, 500, 1000, 2000, 3000, 5000, 8000 and 10 000 hours the furnace was switched off and cooled to room temperature. One specimen of each alloy was taken out of the furnace and used for the analysis. The reacting gas was synthetic air with 25 vol.% CO_2. The gas flow was controlled by a flow meter and the velocity of flow was 2 l/h.

To investigate the chromate formation on high alloy steels, experiments with a similar set up were undertaken (s. Fig. 2b). Five grams of mixed carbonates together with $LiAlO_2$ were put in a melting-pot made of pure alumina. Two nickel foils with the metallic specimen in between were placed vertically in the melting-pot and exposed for 100, 250, 500 and

1000 hours. One crucible was filled only with nickel foils to measure the Cr-impurities dissolved from the technical Ni-foil, from the $LiAlO_2$ and the carbonates. After several periods of time the crucibles were placed into demineralised water, the solution was heated to 70 °C for half an hour and filtered. Under these conditions no Cr^{3+} ions should be in the filtrate, as $Cr(OH)_3$ is nearly insoluble in a basic hydrous solution. The amount of Cr^{6+} (in form of chromates CrO_4^{2-}) in the melt was measured by ICP-OES (inductively coupled plasma-optical emission spectroscopy).

3 Results and discussion

3.1 Results of exposure tests

Figure 3 shows a logarithmic plot of oxide scale thicknesses on the metallic materials after 50, 500 and 1000 hours of exposure. In addition long time exposure tests up to 10 000 hours were conducted on some steels in order to test the long time stability of the scale. The measured scale thicknesses and fit-function of scale growth are shown for three high alloy austenitic steels in Fig. 4. Table 3 lists all corrosion products detected by XRD after several hours of exposure.

3.1.1 Low alloy ferritic steels

The low alloy ferritic steel 1.7380 (10 CrMo 9 10) exhibits very severe corrosion. Mainly nonprotective iron oxides, an inner Fe_3O_4 layer and an outer Fe_2O_3 layer are formed. As Fe_2O_3 is in contact with the eutectic mixture, it reacts with the carbonate melt to form $LiFe_5O_8$. According to the acid-base theory of *Lux* [13] and *Flood, Forland* and *Motzfeld* [14] for molten oxidic salts the carbonate melt is in equilibrium with Li_2O and CO_2:

$$Li_2CO_3 \rightleftharpoons Li_2O + CO_2 \quad (4)$$

The Fe_2O_3, which is in contact with the melt, reacts with Li_2O to form $LiFe_5O_8$ according to Eqn. 5,

$$5Fe_2O_3 + Li_2O \rightleftharpoons 2LiFe_5O_8 \quad (5)$$

$LiFe_5O_8$ has a cubic spinel type crystal structure and is closely related to magnetite (Fe_3O_4). Fifty percent of the

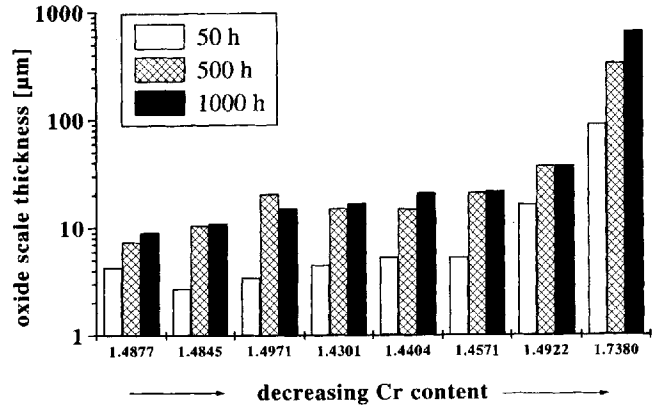

Fig. 3. Measured scale thicknesses of low and high alloy steels after different exposure times in a logarithmic plot

Abb. 3. Logarithmische Auftragung der beobachteten Korrosionsschichtdicken auf niedrig- und hochlegierten Stählen nach verschiedenen Versuchszeiten

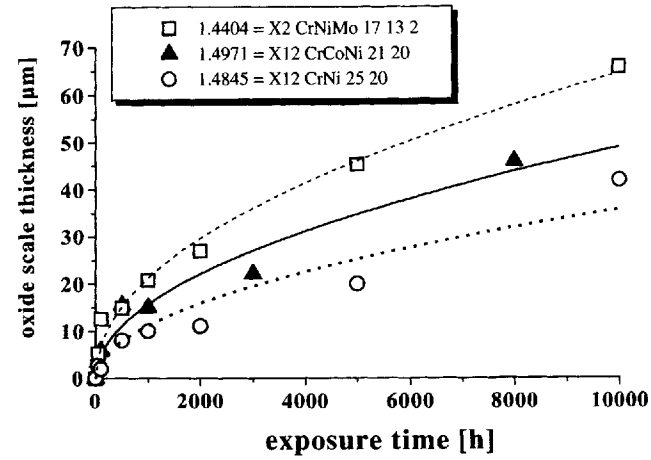

Fig. 4. Oxide scale thickness and fit-functions of three high alloy steels with Cr contents between 17 and 25 wt.% Cr

Abb. 4. Beobachtete Korrosionsschichtdicken dreier hochlegierter Stähle mit Cr-Gehalten zwischen 17 und 25 wt.% mit berechneten Fitfunktionen

Table 3. List of phases formed on steels with different Cr contents under corrosive conditions. Corrosion products put in braces { } were only detected after short exposure times (50 and 100 h). Oxides in parentheses ( ) were detected up to 500 h exposure time and the oxide in brackets [ ] was only found after long exposure times (≥ 1000 h).

Tabelle 3. Auflistung der unter korrosiven Bedingungen gebildeten Oxide auf kommerziellen Stählen mit verschiedenen Cr-Gehalten. Korrosionsprodukte in geschwungenen Klammern { } wurden nur nach kurzen Versuchszeiten (50 und 100 Stunden) nachgewiesen. Oxide in runden Klammern ( ) wurden nach 500 Stunden Auslagerungsdauer und Oxide in eckigen Klammern [ ] werden erst nach langen Versuchszeiten über 1000 Stunden gefunden

steel	Cr content [wt. %]	solid corrosion products after different hours of exposure
1.7380	2–2.25	Fe_3O_4, (Fe_2O_3), $LiFe_5O_8$ and [$LiFeO_2$]
1.4922	10–12.5	$Fe_{3-x}Cr_xO_4$, (Fe_2O_3) and $LiFeO_2$
1.4571	15.5–18.5	(Fe, Ni)Cr_2O_4, (Fe_2O_3, $LiFe_5O_8$) and $LiFeO_2$
1.4404	16.5–18.5	(Fe, Ni)Cr_2O_4, (Fe_2O_3, $LiFe_5O_8$) and $LiFeO_2$
1.4301	17–19	(Fe, Ni)Cr_2O_4, (Fe_2O_3, $LiFe_5O_8$) and $LiFeO_2$
1.4971	20–22.5	{Cr_2O_3 and Fe_2O_3}, $LiCrO_2$, $LiFe_{1-x}Cr_xO_2$, $LiFeO_2$ and [$LiCoO_2$]
1.4845	24–26	{Cr_2O_3 and Fe_2O_3}, $LiCrO_2$, $LiFe_{1-x}Cr_xO_2$ and $LiFeO_2$
1.4877	26–28	{Cr_2O_3 and Fe_2O_3}, $LiCrO_2$, $LiFe_{1-x}Cr_xO_2$, and $LiFeO_2$

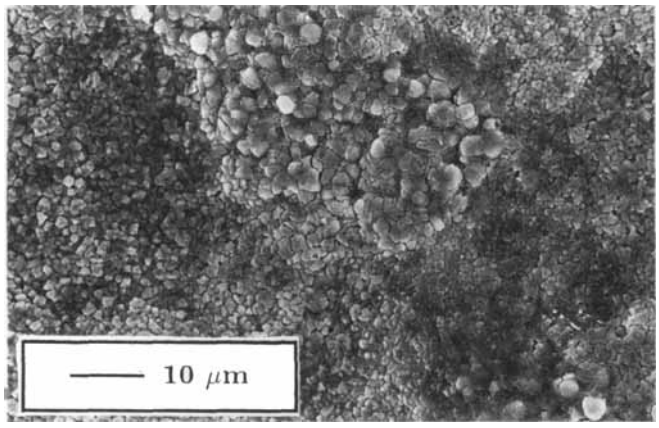

Fig. 5. SEM micrograph of a corroded surface of 1.7380 (10 CrMo 9 10) after 500 hours of exposure

Abb. 5. REM-Bild einer korrodierten Oberfläche von 1.7380 (10 CrMo 9 10) nach 500 Stunden Auslagerungszeit

Fe^{2+} ions in the magnetite structure are replaced by Li^+ ions and 50 percent are replaced by Fe^{3+} ions. The Fe^{3+} ions occupy an eighth of all tetrahedral positions whereas the Li^+ and the remaining Fe^{3+} ions occupy 50 percent of all octahedral gaps in the spinel structure. The structure of $LiFe_5O_8$ can be described as $Fe^{3+}_{tetr.}[Li^+_{0,5}Fe^{3+}_{1,5}]_{oct.}O_4$ [15]. Figure 5 is a SEM micrograph of a surface of corroded 1.7380 after 500 hours of exposure, showing poorly crystallized and nonprotective $LiFe_5O_8$ as an outer scale.

After 5000 h $LiFeO_2$ was detected by XRD, which was formed by lithiation of $LiFe_5O_8$:

$$LiFe_5O_8 + 2Li_2O \rightleftharpoons 5LiFeO_2 \quad (6)$$

The 2.25Cr-1Mo-steel (1.7380) does not fulfil the requirements necessary for cathode current collectors, because fast growing oxides, Fe_3O_4 and $LiFe_5O_8$ (with $LiFeO_2$ after 5000 hours of exposure), are formed.

The ferritic steel 1.4922 (X20 CrMoV 12 1) shows better corrosion resistance than 1.7380 by forming thinner corrosion scales. The Cr content over 10 wt.% Cr leads to the formation of $Fe_{3-x}Cr_xO_4$ as an inner corrosion layer with a Cr content between 14 and 20 wt.% Cr (measured by EDX). The outer hematite layer reacts with Li_2O, but in contrast to 1.7380 (10 CrMo 9 10) $LiFeO_2$ is formed after short exposure times.

$$Fe_2O_3 + Li_2O \rightleftharpoons 2LiFeO_2 \quad (7)$$

$LiFeO_2$ has a rock salt structure with a statistical distribution of Li^+ and Fe^{3+} ions on octahedral sites. The solubility of $LiFeO_2$ in the melt is very low. *Hsu, DeVan* and *Howell* observed a solubility of 78 wppm [16], which was independent of the CO_2 partial pressure. *Shores* and *Qu* [17] observed acidic and basic dissolution of $LiFeO_2$. At high CO_2 partial pressure (≥ 0.5 atm CO_2). $LiFeO_2$ is dissolved by acidic dissolution:

$$LiFeO_2 + 2CO_2 \rightleftharpoons Li^+ + Fe^{3+} + 2CO_3^{2-} \quad (8)$$

At low partial pressure ($\leq 7.1 \cdot 10^{-3}$ atm CO_2) basic dissolution was observed:

$$LiFeO_2 \rightleftharpoons Li^+ + FeO_2^- \quad (9)$$

The lowest solubility occurs in the transient range between $7.1 \cdot 10^{-3}$ and 0.5 atm CO_2 and was determined to be less than 1 mol ppm. The gas atmosphere in these experiments represents the region with low solubility, so that $LiFeO_2$ protects the metal from corrosive attack by the melt. In comparison with 1.7380, the low Cr content in the spinel layer formed on 1.4922 reduces the outward diffusion of iron significantly, but 1.4922 cannot be used as cathode current collector material in MCFC since the scales are growing too fast and a lifetime of 40 000 hours cannot be guaranteed.

3.1.2 High alloy austenitic steels with Cr content ≤ 20 wt.%

When oxidized in air at 650 °C, as in the start of the experiments, the three high alloy austenitic stainless steels (1.4301, 1.4404 and 1.4571) with 16–18 wt.% Cr form mainly iron oxides as an outer scale, whereas spinels (Fe, Ni)Cr_2O_4 are formed as an inner scale in contact with the metal. The superimposed thermodynamic stability diagram of the (Fe-Cr-Ni)-O_2-CO_2-system in Fig. 6 shows that $FeCr_2O_4$ spinel is the stable oxide underneath an Fe_2O_3 layer, which is in equilibrium with the gas atmosphere. At lower oxygen partial pressure Cr_2O_3 is stable in contact with the metallic material, but no Cr_2O_3 was detected on austenitic steels with 16–18 wt.% Cr by XRD or other analytical technics (EPMA or EDX). As the three tested steels show very similar corrosion behavior the following results are applicable to all alloys in this chapter. In addition to corrosion studies marker tests on preoxidized specimens were carried out in order to investigate the growth mechanism of the corrosion scale.

After short exposure times (50 h) Fe_2O_3 and spinel were detected by X-ray diffraction on austenitic steels with 16–18 wt.% Cr. This shows that in the first period mainly attack by air (and not by the melt) takes place. In the period between 50 and 500 h, the corrosion attack by the melt begins and $LiFeO_2$ is formed (Eqn. 7). The well crystallized structure of $LiFeO_2$ formed on 1.4404 after 500 h is shown in Fig. 7

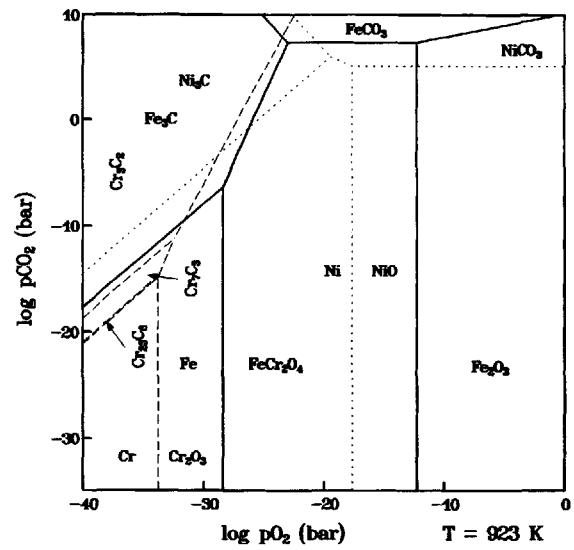

Fig. 6. Superimposed thermodynamic stability diagram of the (Fe-Cr-Ni)-O_2-CO_2 system at 650 °C

Abb. 6. Überlagertes thermodynamisches Stabilitätsdiagramm des Systems (Fe-Cr-Ni)-O_2-CO_2 bei 650 °C

and the microprobe linescan of a cross section of 1.4404 after 500 hours is plotted in Fig. 8. In addition to spinel and $LiFeO_2$ reflections, $LiFe_5O_8$ was detected by XRD on 1.4404 and 1.4571 after 500 hours of exposure. which was formed at the $Fe_2O_3/LiFeO_2$ interface (Eqn. 10).

$$LiFeO_2 + 2Fe_2O_3 \rightleftharpoons LiFe_5O_8 \qquad (10)$$

After 500 h the corrosion scale consists of three oxides: a thin $LiFeO_2$ layer, which is in contact with the liquid carbonate, a (Fe, Ni)Cr_2O_4 spinel layer, which is in contact with the metal and a $LiFe_5O_8$ layer in between. The linescan of 1.4404 after 500 h (Fig. 8) shows that the outer Li containing layers are free of Cr or Mo, whereas the (Fe, Ni)Cr_2O_4 spinel layer contains high amounts of Cr and Mo (2–4 wt.% Mo in the spinel layer). Mn which is a widespread alloying element in stainless steels was detected mainly in the outer areas of the corrosion scale and only small amounts of Mn were found in the spinel layer. Mn diffuses through the spinel layer and is incorporated into $LiFeO_2$.

Au markers, which were vapour deposited on specimens after preoxidation (50 h at 650 °C in 25 vol.% CO_2/air), were found on the $LiFe_5O_8$/spinel interface after 500 hours of exposure (Fig. 9). Obviously the outer oxide layers ($LiFeO_2$ and $LiFe_5O_8$) grow mainly by outward diffusion of iron, whereas the spinel grows by inward diffusion of oxygen. This means that $LiFeO_2$ is formed at the oxide/melt interface by reaction of trivalent iron ions with Li_2O:

$$Fe^{3+} + 2Li_2O \rightleftharpoons LiFeO_2 + 3Li^+, \qquad (11)$$

whereas $LiFe_5O_8$ is formed at the $LiFeO_2/Fe_2O_3$ interface according to Eqn. 10.

After 5000 and 10 000 hours of exposure no $LiFe_5O_8$ layer was detectable. From metallographic cross sections (Fig. 10), XRD and with in an EPMA-linescan (Fig. 11) a double layered corrosion scale was observed, which consists of an outer $LiFeO_2$ layer and an inner spinel layer. The intermediate layer $LiFe_5O_8$ was fully lithiated by inward diffusion of Li^+ ions in the period 500–5000 h:

$$LiFe_5O_8 + 3Li^+ \rightleftharpoons 4LiFeO_2 + Fe^{3+} \qquad (12)$$

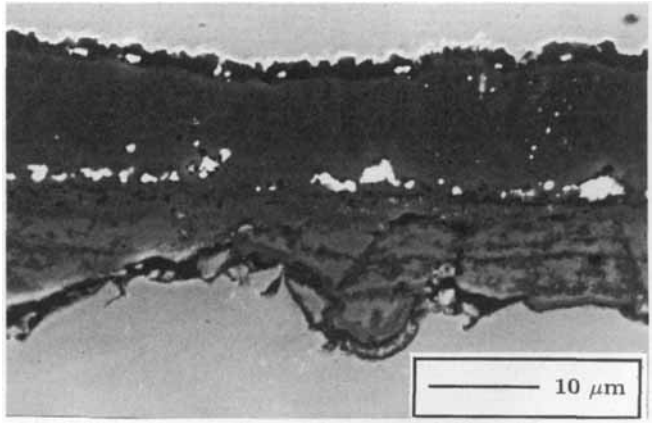

Fig. 7. SEM micrograph of a corroded surface of 1.4404 (AISI 316 L) after 500 hours exposure time. The crystallized $LiFeO_2$ rhombohedra cover the entire surface

Abb. 7. REM-Bild einer korrodierten Oberfläche von 1.4404 (AISI 316 L) nach 500 Stunden Auslagerungszeit. Rhomboedrische Kristalle von $LiFeO_2$ überdecken die gesamte Oberfläche

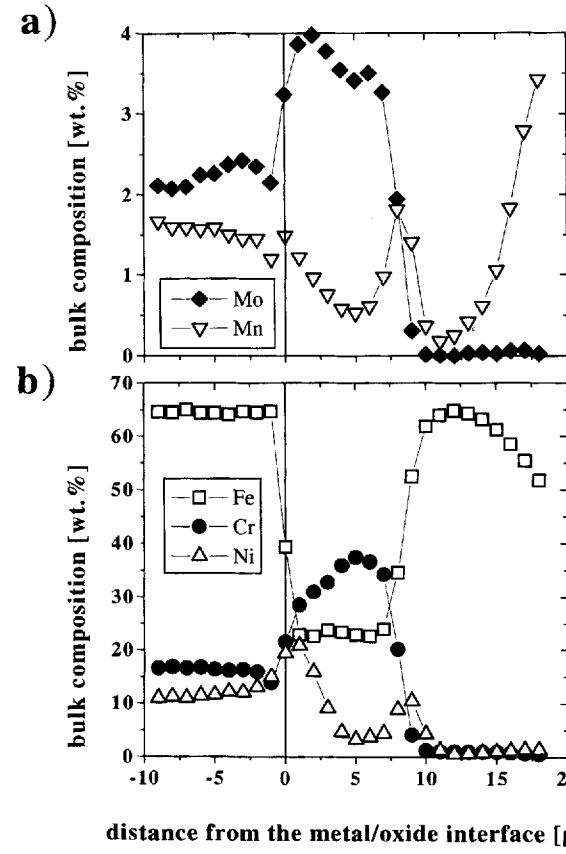

Fig. 8. An EPMA linescan of the corrosion layer of 1.4404 after 500 h: a) Mo and Mn b) Fe, Cr and Ni

Abb. 8. ESMA Linescan durch die Korrosionsschicht des Werkstoffes 1.4404 nach 500 Stunden: a) Mo und Mn b) Fe, Cr und Ni

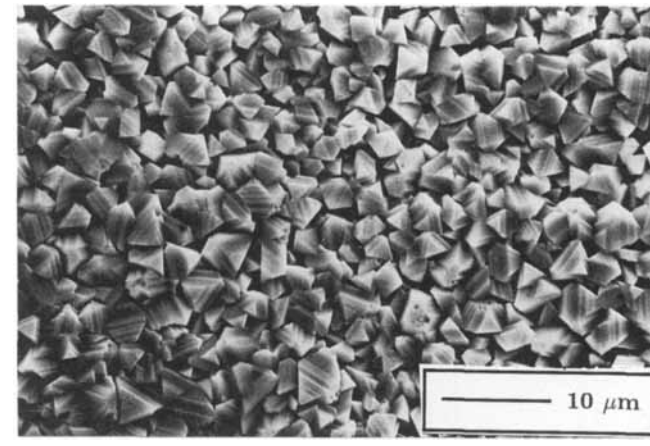

Fig. 9. SEM micrograph of preoxidized specimen of 1.4404 (coated with Au-marker) after 500 hours of exposure. The Au markers are found at the spinel/$LiFe_5O_8$ interface. Obviously the outer iron rich oxides are formed by outward-diffusion of iron cations

Abb. 9. REM-Bild einer voroxidierten Probe des Werkstoffes 1.4404 nach 500 Stunden Auslagerungsdauer. Die Gold-Marker werden an der Spinell/$LiFe_5O_8$ Grenzfläche vorgefunden. Die äußeren, eisenreichen Oxide wachsen überwiegend durch Auswärtsdiffusion von Eisenkationen

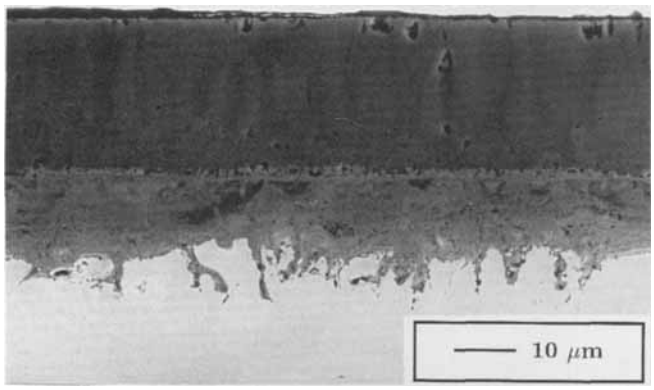

Fig. 10. SEM micrograph of a metallographic cross section of 1.4404 after 5000 hours of exposure. The main corrosion product is $LiFeO_2$ with a mixed $(Fe,Ni)Cr_2O_4$ spinel layer underneath

Abb. 10. REM-Bild eines metallographischen Querschliffes von 1.4404 nach 5000 Auslagerungsstunden. $LiFeO_2$ ist das Hauptkorrosionsprodukt, unter welchem sich eine gemischte $(Fe,Ni)Cr_2O_4$ Spinellschicht befindet

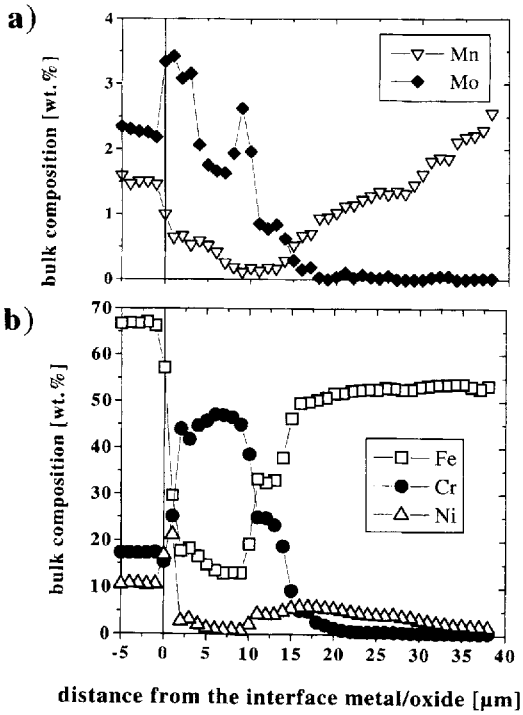

Fig. 11. An EPMA linescan of the corrosion layer of 1.4404 after 5000 h: a) Mo and Mn b) Fe, Cr and Ni

Abb. 11. ESMA-Linescan senkrecht zur Korrosionsschicht des Werkstoffes 1.4404 nach 5000 Stunden: a) Mo und Mn b) Fe, Cr und Ni

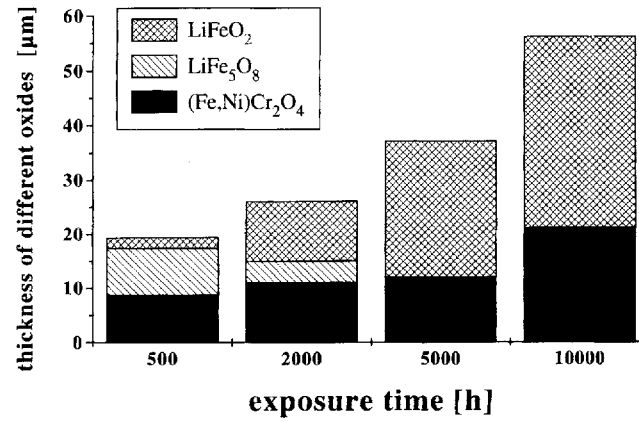

Fig. 12. Schematic construction of the oxide scales of 1.4404 (AISI 316 L) after 500, 2000, 5000 and 10 000 hours of exposure

Abb. 12. Schematischer Aufbau der einzelnen Oxide der Korrosionsschicht gewachsen auf 1.4404 (AISI 316 L) nach 500, 2000, 5000 und 10 000 Versuchsstunden

The trivalent iron cations diffuse to the $LiFeO_2$/melt interface and form $LiFeO_2$ according to Eqn. 11. Figure 12 shows a schematic plot of the oxide scales on 1.4404 after different hours of exposure. $LiFeO_2$ grows most rapidly of all observed oxides, because of fast outward diffusion of Fe^{3+} ions, whereas the spinel layer shows slow growth. The formation of $LiFeO_2$ can be described by four reactions. At first outward diffusing iron cations react with the melt to form $LiFeO_2$. Then the formation of $LiFe_5O_8$ takes place at the newly formed interface $LiFeO_2/Fe_2O_3$ and in a last step Li^+ ions diffuse into the corrosion layer to lithiate $LiFe_5O_8$:

$$2Li_2CO_3 \rightleftharpoons 2Li_2O + 2CO_2$$
$$Fe^{3+} + 2Li_2O \rightleftharpoons LiFeO_2 + 3Li^+$$
$$LiFeO_2 + 2Fe_2O_3 \rightleftharpoons LiFe_5O_8$$
$$LiFe_5O_8 + 3Li^+ \rightleftharpoons 4LiFeO_2 + Fe^{3+}$$

$$\sum: 2Fe_2O_3 + 2Li_2O \rightleftharpoons 4LiFeO_2 + 2CO_2 \quad (13)$$

In a previous paper [18] the authors have presented a mechanism for these changes in the composition of the corrosion scales after different hours of exposure and provide a mechanism for the spinel growth.

3.1.3 High alloy austenitic steels with Cr content ≥ 20 wt.%

In oxidizing atmospheres at high temperatures (T ≥ 700 °C) a high Cr content in austenitic steels usually leads to the formation of a protective Cr_2O_3 layer, which prevents the metal from further oxidation. However Cr_2O_3 is not stable in liquid carbonate and in direct contact with the melt it is oxidized to chromates (Eqn. 15) by peroxide ions which are formed at the melt/gas interface (Eqn. 14):

$$CO_3^{2-} + \frac{1}{2}O_2 \rightleftharpoons CO_2 + O_2^{2-} \quad (14)$$

$$Cr_2O_3 + 3O_2^{2-} \rightleftharpoons 2CrO_4^{2-} + O^{2-} \quad (15)$$

Steels with high Cr content ≥ 20 wt.% Cr such as 1.4971 (X20 CrCoNi 21 20), 1.4845 (X12 CrNi 25 20) and 1.4877 (X5 NiCrNbCe 32 27), form large amounts of chromate, which is highly soluble in the melt. The solubility of mixed $(Li,K)_2CrO_4$ in $(Li_{0.62}K_{0.38})_2CO_3$ melt was determinated by *Hsu, DeVan* and *Howell* to be 13.7 wt.% [16]. Figure 13 shows a corroded surface of 1.4845 (SS 310S) after 5000 hours of exposure and large areas of solidified chromates are visible. The reaction of Cr_2O_3 to soluble chromates

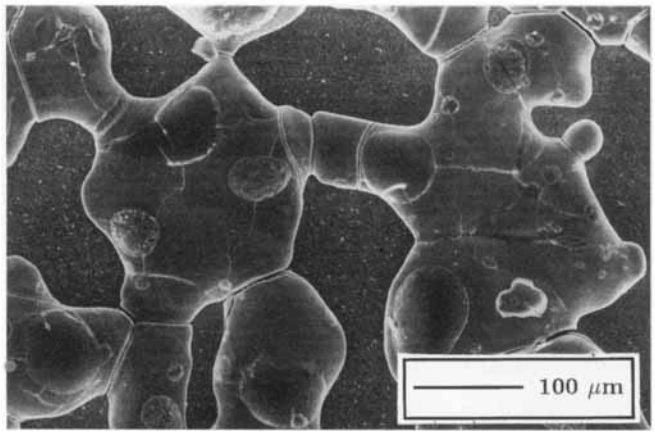

Fig. 13. SEM micrograph of a corroded surface of 1.4845 (AISI 310 S) after 5000 hours exposure time. Large amounts of solidified chromates are still visible

Abb. 13. REM-Bild einer korrodierten Oberfläche von 1.4845 (AISI 310 S) nach 5000 Stunden Auslagerungszeit. Große Mengen erstarrten Chromates sind auf der Oberfläche sichtbar

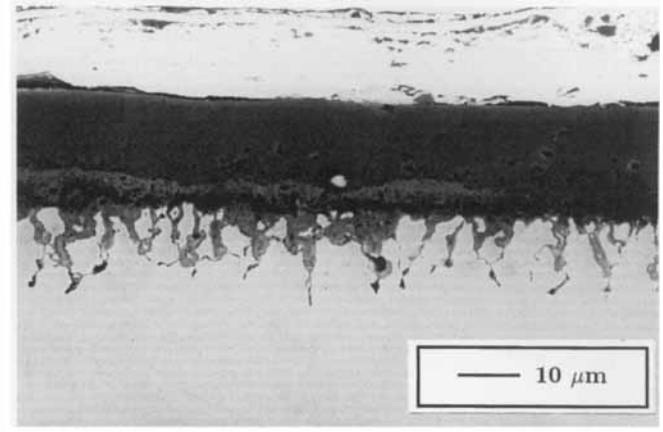

Fig. 14. SEM micrograph of a metallographic cross section of 1.4845 after 5000 hours of exposure time. A mixed $(Fe, Cr)_2O_3$ was detected with EPMA under the corrosion scale at the grain boundaries, whereas $LiCrO_2$, mixed $LiCr_{1-x}Fe_xO_2$ and $LiFeO_2$ were detected by XRD

Abb. 14. REM-Bild eines metallographischen Querschliffes des Werkstoffes 1.4845 nach 5000 Versuchsstunden. Ein gemischtes $(Fe, Cr)_2O_3$ Oxid wurde mit ESMA entlang der Korngrenzen gefunden, während $LiCrO_2$, $LiCr_{1-x}Fe_xO_2$ und $LiFeO_2$ mit röntgenographischen Methoden nachgewiesen wurden

leads to outward transport of Cr and hinders the formation of a protective Cr_2O_3 scale. In addition, a large electrolyte loss due to Eqns. 14 and 15 is associated with the formation of chromates. Chromates are more basic than carbonates and with their formation oxygen ions are liberated, so the melt becomes more basic (Eqn. 15).

Along with soluble chromates, the tested chromium rich steels form Fe_2O_3 and Cr_2O_3 in the initial stages of the corrosion process. After 50 hours of exposure Fe_2O_3 and Cr_2O_3 were detected by XRD, but after several hundred hours of exposure, Fe_2O_3 is converted to $LiFeO_2$, whereas the inner Cr_2O_3 scale is transformed to $LiCrO_2$:

$$Cr_2O_3 + Li_2O \rightleftharpoons 2LiCrO_2 \qquad (16)$$

Figure 14 shows a cross section of the scale on 1.4845 and Fig. 15 shows an EPMA linescan after 5000 hours of exposure. The oxide scale consists of an outer $LiFeO_2$ and an inner $LiCrO_2$ layer. Between these two oxides a 10 µm thick region exists, where the iron content increases outward and the chromium content decreases. As shown by *Kordes* and *Petzold* [19], $LiFeO_2$ and $LiCrO_2$ form a continuous row of mixed crystals $LiCr_{1-x}Fe_xO_2$. Cubic symmetry was observed at high Fe content, whereas hexagonal symmetry was observed at high Cr content. Half way between $LiFeO_2$ and $LiCrO_2$ a layer was observed on 1.4845 which consists of $LiCr_{1-x}Fe_xO_2$ determinated by EPMA. The formation of $LiCr_{1-x}Fe_xO_2$ and the Cr rich oxide $LiCrO_2$ below the $LiFeO_2$ scale explains the thinner corrosion scales of the chromium rich steels compared to spinel forming steels with lower Cr content. *Yuh* found that the Cr rich inner oxide limits the cation diffusion and hence the overall corrosion rate [8].

A high Co content in high alloy austenitic steels leads to the formation of an additional oxide. The stable oxide of pure Co in oxidizing atmospheres at 650 °C is Co spinel Co_3O_4 (see the thermodynamic stability diagram of Co in Fig. 16). In contact with carbonate melt, Co_3O_4 is oxidized to $LiCoO_2$ [20]:

$$2Co_3O_4 + 3Li_2CO_3 + \frac{1}{2}O_2 \rightleftharpoons 6LiCoO_2 + 3CO_2 \qquad (17)$$

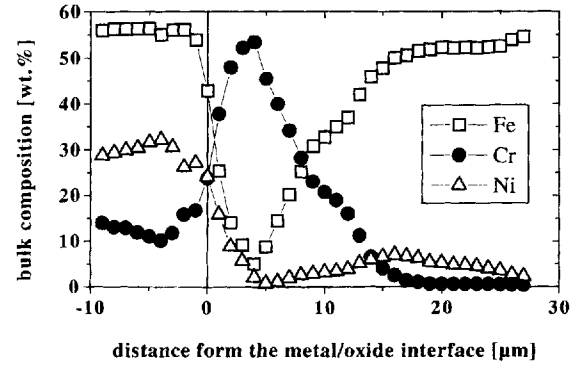

Fig. 15. An EPMA linescan of the corrosion layer of 1.4845 after 5000 hours of exposure

Abb. 15. Ein ESMA-Linescan senkrecht zur Korrosionsschicht des Stahles 1.4845 nach 5000 Versuchsstunden

After 500 hours the high Co containing steel 1.4971 (X20 CrCoNi 21 20) forms $LiFeO_2$ with significant amounts of dissolved Co (s. Fig. 17). However a Co containing $LiFeO_2$ is not stable as we have observed. Co diffuses outward to the melt/scale interface and flat crystals of a Co rich oxide are formed (Figs. 18 and 19). After 8000 hours of exposure the whole surface of 1.4971 is covered with flat crystals (s. Fig. 21) which are determined by XRD and microprobe analysis to be $LiCoO_2$. A SEM micrograph of a metallographic cross section after 3000 hours of exposure is shown in Fig. 20, the corresponding linescan is given in Fig. 22. The formation of $LiCoO_2$ can be described as a demixing reaction of Co containing $LiFeO_2$:

$$LiFe_{1-x}Co_xO_2 \Longrightarrow LiFe_{1-x+y}O_2 + yLiCoO_2 \qquad (18)$$

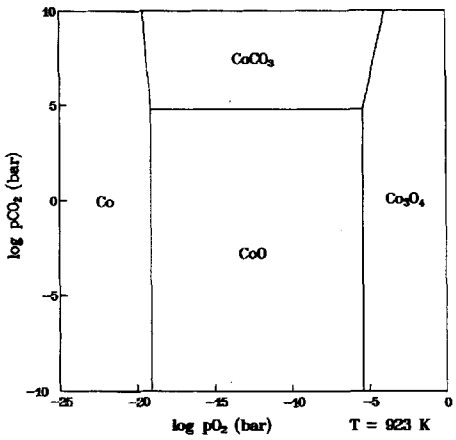

Fig. 16. Thermodynamic stability diagram of the system Co-O-CO_2 at 650 °C. In usual MCFC-gas mixtures with (15–25 vol.% CO_2 with 15–25 vol.% O_2 (bal. N_2)) Co-spinel is the stable oxide

Abb. 16. Thermodynamisches Stabilitätsdiagramm des Systems Co-O-CO_2 bei 650 °C. In üblichen MCFC-Kathodengasgemischen (15–25 vol.% CO_2 und 15–25 vol.% O_2; Rest N_2) stellt Co-Spinell das stabile Oxid dar

Fig. 17. SEM micrograph of a corroded surface of 1.4971 after 500 hours of exposure. $LiFeO_2$ containing Co (right side) is covered by K_2CrO_4 on the left side

Abb. 17. REM-Bild einer korrodierten Oberfläche von 1.4971 nach 500 Stunden Auslagerungszeit. Co-haltiges $LiFeO_2$ (rechts) wird überdeckt von erstarrtem K_2CrO_4 (links)

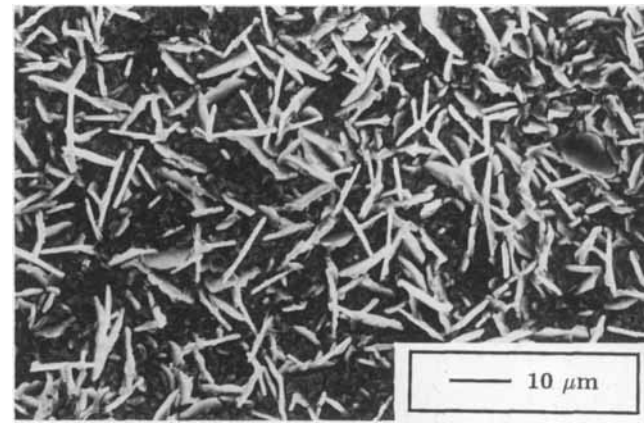

Fig. 18. SEM micrograph of a corroded surface of 1.4971 after 1000 h: Needle-shaped crystals of $LiCoO_2$ are recognizable

Abb. 18. REM-Bild einer korrodierten Oberfläche von 1.4971 nach 1000 Stunden Auslagerungszeit: Nadelförmige Kristalle von $LiCoO_2$ sind sichtbar

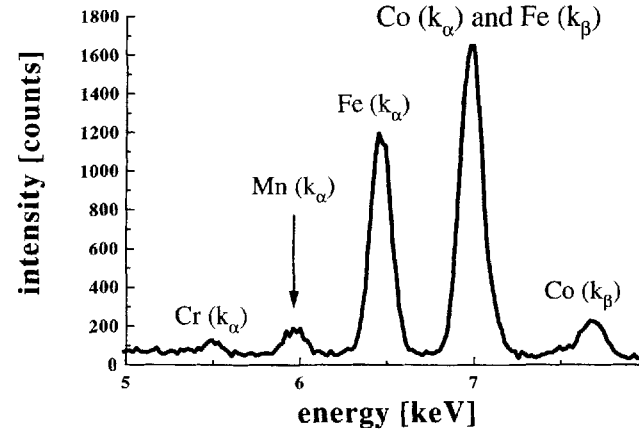

Fig. 19. EDX-Spectra of the surface of 1.4971 (X12 CrCoNi 21 20) after 1000 hours of exposure

Abb. 19. EDX-Spektrum der Oberfläche des Stahles 1.4971 (X12 CrCoNi 21 20) nach 1000 Stunden Auslagerungsdauer

with $x \neq y$. Co doped $LiFeO_2$ demixes to a less Co doped $LiFeO_2$ with an overgrown $LiCoO_2$ layer. $LiCoO_2$ has rock salt structure and is very similar to $LiFeO_2$. In the last decades $LiCoO_2$ has become an alternative cathode material for fuel cells, because the solubility of $LiCoO_2$ in the eutectic carbonate melt is much lower than the solubility of the normally used cathode material NiO(Li). *Veldhuis* [21] and *Plomb* [22] observed a dissolution rate of 0.5 µg/cm² h for $LiCoO_2$ which is eight times lower than the dissolution rate for NiO (4 µg/cm² h), so that $LiCoO_2$ can act as a protective, less soluble oxide layer in carbonate melts.

3.2 Investigations on the total corrosion

The total corrosion rate is the result of two different processes, i.e., the metal loss caused by the formation of solid oxides and by the formation of chromates. Chromate formation diminishes the total mass of the stainless steel, whereas formation of solid oxides leads to an increasing mass change. Therefore, the mass gain caused by the formation of solid oxides is not equal to the mass gain of a metallic, washed and dried specimen before and after the experiment. With regard to the mass loss by chromate formation, the observed mass gain can be written as:

$$\Delta m_{obs.} = m_{t=x} - m_{t=0} = m_{O+Li} - m_{Cr^{6+}} \quad (19)$$

where:

$\Delta m_{obs.}$: observable mass gain of washed and dried specimen before and after the experiment
$m_{t=x}$: mass of specimen after the experiment
$m_{t=0}$: mass of specimen before the experiment

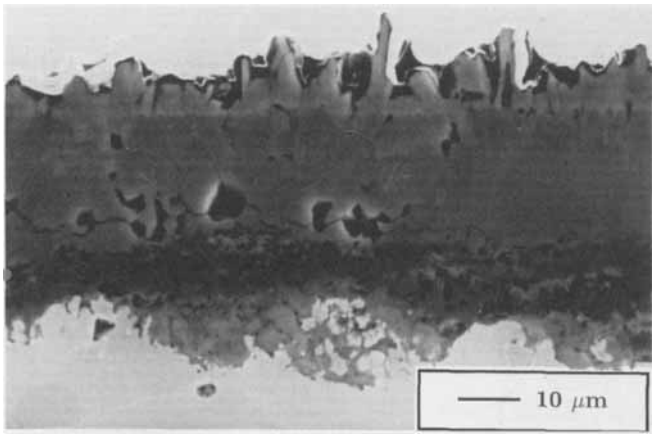

Fig. 20. SEM micrograph of a cross section of 1.4971 (X12 CrCoNi 21 20) after 3000 hours of exposure. The corrosion scale consists of an inner $LiCrO_2$, $LiFeO_2$ and $LiCoO_2$ on top of the scale. Flat crystals of $LiCoO_2$ are also visible in the cross section

Abb. 20. REM-Bild eines Querschliffs des Werkstoffes 1.4971 (X12 CrCoNi 21 20) nach 3000 Stunden Auslagerungszeit. Die Korrosionsschicht besteht aus einer inneren $LiCrO_2$-Schicht sowie $LiFeO_2$ und $LiCoO_2$, welches auf $LiFeO_2$ gewachsen ist. Die kantigen Kristalle von $LiCoO_2$ sind auch im Querschliff sichtbar

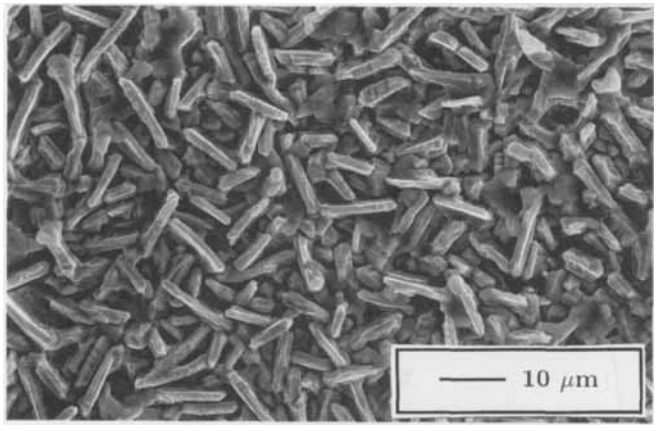

Fig. 21. SEM micrograph of a corroded surface of 1.4971 after 8000 h: The whole surface consists of flat crystals of $LiCoO_2$

Abb. 21. REM-Bild einer korrodierten Oberfläche von 1.4971 nach 8000 Stunden Auslagerungszeit: Die gesamte Oberfläche besteht aus $LiCoO_2$-Kristallen

m_{O+Li}: mass gain caused by the assimilation of oxygen and lithium (formation of insoluble, solid oxides like $LiCrO_2$, spinels, $LiFeO_2$ and $LiCoO_2$)

$m_{Cr^{6+}}$: mass of detected chromium in the melt

The sum of observed mass gain and the mass of K_2CrO_4 can be expressed as *total corrosion mass gain*, considering all corrosion products:

$$\Delta m_{total\ corrosion} = m_{obs.} + m_{K_2CrO_4} \qquad (20)$$

Stainless steels form different corrosion products depending on their composition. As already shown, low alloy steels form mainly insoluble Li-Fe-oxides, whereas steels with high Cr content form thin corrosion scales and also K_2CrO_4, which

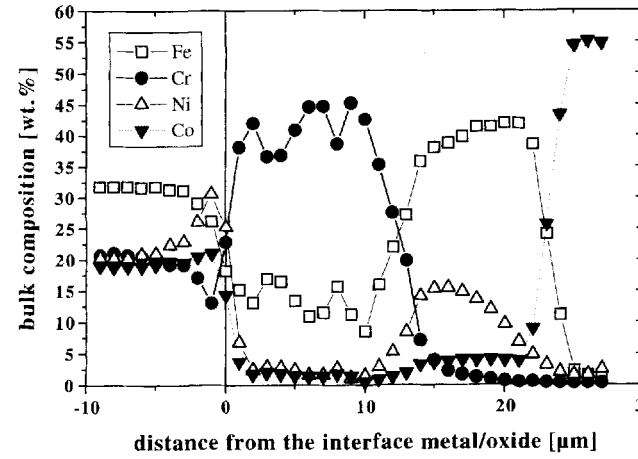

Fig. 22. EPMA linescan of 1.4971 (X12 CrCoNi 21 20) after 3000 hours of exposure. The corrosion scale consists of three oxides: an outer $LiCoO_2$-scale and an inner $LiCrO_2$-scale with a Ni rich $LiFeO_2$ in between

Abb. 22. ESMA-Linescan senkrecht zur Probenoberfläche des Werkstoffes 1.4971 (X12 CrCoNi 21 20) nach 3000 Stunden Auslagerungszeit. Die Korrosionsschicht besteht aus drei verschiedenen Oxiden: einer äußeren $LiCoO_2$- und einer inneren $LiCrO_2$-Schicht. Zwischen diesen beiden Oxiden wird eine Ni-reiche $LiFeO_2$-Schicht beobachtet

is highly soluble in liquid carbonate. Figure 23 shows the surface of AC66 (1.4877) after 50 h of exposure covered with K_2CrO_4 which has been formed on the scale surface after cooling. Solidified K_2CrO_4 was detected on all steels with high Cr content by XRD and EDX, whereas Li_2CrO_4 reflections were not observed. The formation of K_2CrO_4 can be explained by the reaction of Cr_2O_3 with peroxide ions as already shown in Eqn. 15 and solidification upon cooling. The extent of chromate formation and therefore the total metal loss by corrosion is not considered in measurements of the corrosion scale thickness. In order to quantify the chromate formation and the total mass gain by formation of solid corrosion products exposure tests on four commercial steels with Cr contents

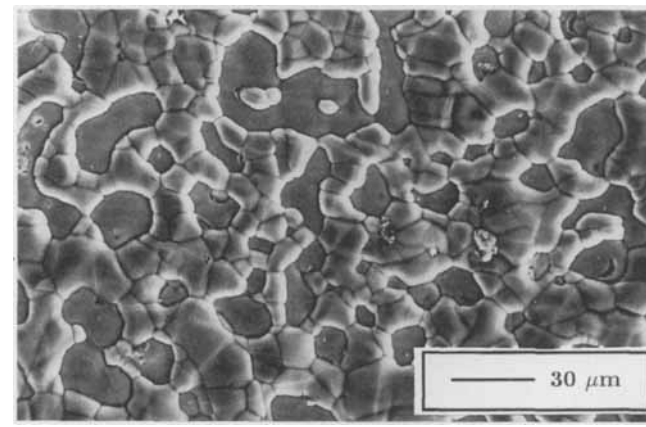

Fig. 23. SEM micrograph of a corroded surface of 1.4877 (AC 66) after 50 hours exposure time, K_2CrO_4 is the main corrosion product and covers most of the surface

Abb. 23. REM-Bild einer korrodierten Oberfläche von 1.4877 (AC 66) nach 50 Stunden Auslagerungszeit. K_2CrO_4 stellt das wichtigste Korrosionsprodukt dar und bedeckt größtenteils die Oberfläche

Table 4. Steels used for the total corrosion experiments with Cr-content, structure, amounts of reactive elements (in wt.%) and molar fraction of Cr. $\left(x_{Cr} = \frac{n(Cr)}{n(Fe)+n(Cr)+n(Ni)+...}\right)$

Tabelle 4. Stähle, die für die Untersuchungen zur gesamten Korrosion, Cr-Gehalt, Struktur, Zusätzen an reaktive Elementen (in Gew.%) und Cr-Molenbruch $\left(x_{Cr} = \frac{n(Cr)}{n(Fe)+n(Cr)+n(Ni)+...}\right)$ verwendet wurden

steel	Cr [wt.%]	reactive elements [wt.%]	structure	Cr molar fraction
1.4922	10–12.5	0.8–1.2 Mo; 0.27–1.25 V	ferritic	11.8
1.4404	16.5–18.5	2–2.5 Mo	austenitic	18.3
1.4971	20–22.5	2.5–3.5 Mo; 2–3 W; 0.75–1.25 Nb	austenitic	23.5
1.4877	26–28	0.6–1.0 Nb; 0.05–0.1 Ce	austenitic	27.9

from 12–27 wt.% Cr with different amounts of reactive elements (Table 4) were carried out with a vertical setup (Fig. 2 b). The measured mass gain after 100, 250, 500 and 1000 hours of exposure of washed and dried specimens before and after the experiment and the amounts of Cr^{6+}, which was found in the carbonate melt and detected by chemical analysis, are plotted in Fig. 24 and Fig. 25. Figure 24 shows that the measured mass gain by assimilation of oxygen and lithium decreases with increasing Cr content. As already shown above high alloy steels form highly Cr containing oxides (mainly $LiCrO_2$ and $LiCr_{1-x}Fe_xO_2$) which reduce the outward diffusion of Fe^{3+} ions and limit the formation of solid, less soluble $LiFeO_2$. The main corrosion product of high alloy steels is also liquid chromate, which is not considered in the measurements of the oxide scale thickness. The amount of Cr^{6+} ions in the melt after different times is shown in Fig. 25. Figure 24 and Fig. 25 show contrary effects. Naturally increasing Cr content leads to increasing chromate formation, decreasing Cr content leads to increasing mass gain by formation of different oxides.

The *total corrosion mass gain* of the four tested high alloy steels (calculated with Eqn. 20) is shown in Fig. 26. The total corrosion mass gain shows that 1.4404 with 17 wt.% Cr is the best material. Higher Cr content leads to increasing formation of chromates connected with electrolyte loss, whereas steels with lower amounts of chromium form an inner spinel layer which does not reduce the outward diffusion of iron ions in that way, that fast growing iron oxides were not formed.

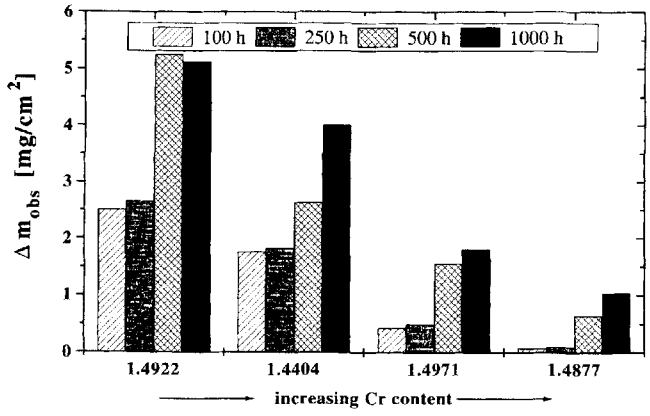

Fig. 24. Observed mass gain of washed and dried specimens before and after 100, 250, 500 and 1000 hours of exposure. Low alloy steels with Cr-contents under 20 wt.% Cr (1.4922 and 1.4404) form mainly solid oxides ($LiFeO_2$ and spinels)

Abb. 24. Beobachtete Massenzunahmen von gewaschenen und getrockneten Proben (aufgelistet nach steigendem Cr-Gehalt) nach 100, 250, 500 und 1000 Stunden Auslagerungsdauer. Niedriglegierte Stähle mit Cr-Gehalten unter 20 Gew.-% Cr (1.4922 und 1.4404) bilden überwiegend feste Oxide ($LiFeO_2$ und Spinelle) aus

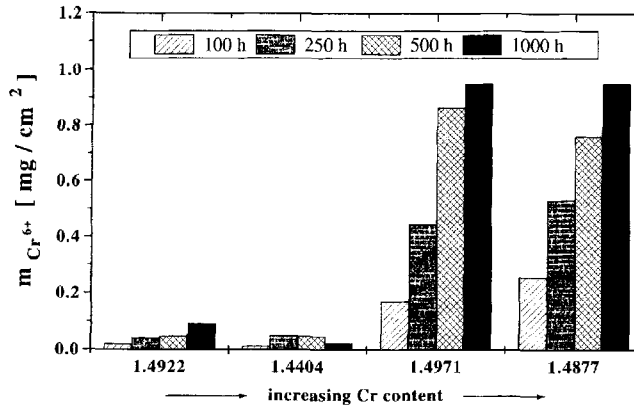

Fig. 25. Observed Cr^{6+} content of the melt of four alloy steels (listed with increasing Cr-Content) after 100, 250, 500 and 1000 hours of exposure. The high alloy steels 1.4971 and 1.4877 form mainly chromates

Abb. 25. Beobachteter Cr^{6+}-Gehalt der Schmelze (aufgelistet nach steigendem Cr-Gehalt der Stähle) nach 100, 250, 500 und 1000 Auslagerungsstunden. Die hochlegierten Stähle 1.4971 und 1.4877 bilden überwiegend leicht lösliche Chromate

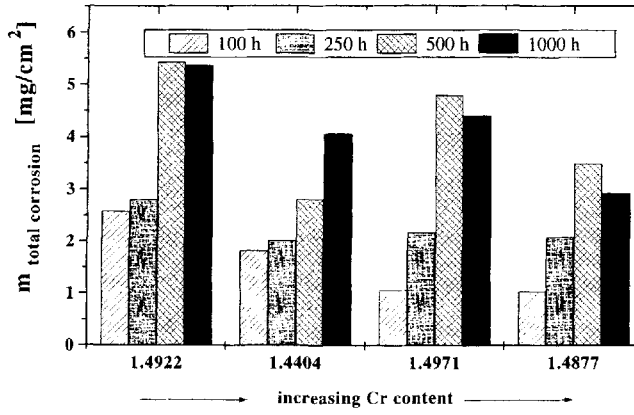

Fig. 26. Total mass of corrosion products of four high alloy steels after 100, 250, 500 and 1000 hours of exposure

Abb. 26. Gesamtmasse aller Korrosionsprodukte der vier Stähle nach 100, 250, 500 und 1000 Auslagerungsstunden

4 Summary

The corrosion behavior of low and high alloy steels was tested under simulated molten carbonate fuel cell conditions as present in the cathodic area. The low alloy steel 1.7380 (10 CrMo 9 10) forms porous oxide layers of Fe_3O_4 and $LiFe_5O_8$ in contact with the melt and exhibits poor corrosion protection. $LiFeO_2$ and $Fe_{3-x}Cr_xO_4$ spinel layers are formed on steels with Cr contents between 10 and 20 wt.% Cr. Increasing Cr content in the alloy leads to increasing Cr content in the spinel layer. $LiFeO_2$ is nearly insoluble in the melt and retards further corrosive attack by the carbonate melt. Marker tests have shown, that the $LiFeO_2$ layer grows by outward diffusion of iron, whereas the inner spinel layer grows mainly by inward diffusion or transport of oxygen. $LiFeO_2$ containing much Co, which was found on 1.4971 (X12 CrCoNi 21 20) after 500 h, is subject to a demixing phenomenon, $LiCoO_2$ was formed above such layer after several thousand hours of exposure. Steels with Cr contents of over 20 wt.% form Fe_2O_3 and Cr_2O_3, which are converted to $LiFeO_2$ and $LiCrO_2$ with time. The $LiCrO_2$ scale limits the outward diffusion of iron cations and the growth of the corrosion scale.

The chromate formation was studied on four steels with Cr content between 12 and 27 wt.% Cr. Steels with Cr content of over 20 wt.% form mainly dissolved chromate, whereas steels with less than 20 wt.% Cr form mainly solid, less soluble oxides. The sum of soluble chromate and formation of solid, less soluble oxides is called *total corrosion*. The total corrosion shows that steels with Cr contents of 17 wt.% Cr are the best choice for current collector materials. Materials with lower Cr content form fast growing oxides, whereas a higher Cr content leads to the formation of soluble chromate, as which is the main corrosion product.

5 Acknowledgment

The support of this work under contract no. 0329173B from the BMBF (Bundesministerium für Bildung, Wissenschaft, Forschung und Technologie) is gratefully acknowledged.

6 References

[1] *W. Gajewski:* Phys. Bl. *50* (1994) 560.
[2] *H. Kettler:* VDI-Nachrichten *21* (1995) 19.
[3] *D. A. Shores, M. Pischke:* Proceedings of the Third International Symposium on Carbonate Fuel Cell Technology 93-3, Electrochemical Soc. (1993) p. 214.
[4] *H. S. Hsu, J. H. DeVan, M. Howell:* J. Electrochem. Soc. *134* (1987) 3038.
[5] *G. J. Janz, A. Conte:* Corrosion *20* (1964) 327.
[6] *G. J. Janz, A. Conte:* Electrochim. Acta *9* (1964) 1279.
[7] *D. A. Shores, P. Singh:* Proc. Electrochem. Soc. 94-13, Pennington N. J. USA (1984). Electrochem. Society, p. 271–296.
[8] *C. Yuh, R. Johnson, M. Farooque, H. Maru:* Proc. Electrochem. Soc. 93-3, Electrochemical Soc. (1993) p. 158–170.
[9] *C. Yuh:* Proc. Electrochem. Soc. 90-16, Electrochemical Soc. (1990) S. 368–373.
[10] *W. A. El Rahem Ghanem:* Steel Res. *64* (1993) 317.
[11] *P. Singh, H. C. Maru:* Corrosion '85, NACE (1985) Paper 334.
[12] VDEh. Stahl-Eisen-Liste, Verlag Stahleisen, Düsseldorf 1993.
[13] *H. Lux:* Z. Elektrochem. angew. phys. Chemie *45* (1939) 303.
[14] *H. Flood, T. Forland, K. Motzfeld:* Acta chem. Scand. *6* (1952) 257.
[15] *N. N. Greenwood:* Ionenkristalle, Gitterdefekte und Nichtstöchiometrische Verbindungen. Verlag Chemie, Weinheim 1985.
[16] *H. S. Hsu, J. H. DeVan, M. Howell:* J. Electrochem. Soc. *134* (1987) 2146.
[17] *D. A. Shores, Y. Qu:* Proceedings of the Third International Symposium on Carbonate Fuel Cell Technology 93-3, Electrochemical Soc. (1993) 356–367.
[18] *M. Spiegel, P. Biedenkopf, H. J. Grabke:* Corr. Sci. *39* (1997) 1193.
[19] *E. Kordes, L. Petzold:* Zeit. anorg. allgem. Chemie *335* (1965) 138.
[20] *A. Lundblatt, B. Bergmann:* Proceedings of the First International Symposium on New Materials For Fuel Cell Systems 1. Le Laboratoire d'électochimie et de matériaux énergétitique École Polytechnique de Montréal (1995).
[21] *J. B. J. Veldhuis, E. C. Eckes, L. Plomb:* J. Electrochem. Soc. *139* (1) (1992) L6–L8.
[22] *L. Plomb, J. R. Veldhuis, E. F. Sitters, S. B. V. der Molen:* J. Power Sources *39* (1992) 369.

(Received: January 8, 1997) W 3186